Cellulose (2025) 32:211–227
https://doi.org/10.1007/s10570-024-06291-z

ORIGINAL RESEARCH

Influence of magnetic nanoparticles on the mechano-magnetic response of wet-spun sodiumalginate-nanocellulose filaments

Lisandra de Castro-Alves · Ling Wang · Manuel A. González-Goméz · Pelayo Garcia-Acevedo · Ángela Arnosa-Prieto · Maryam Borghei · Yolanda Piñeiro-Redondo · Orlando J. Rojas · José Rivas

Received: 23 May 2024 / Accepted: 9 November 2024 / Published online: 16 November 2024
© The Author(s) 2024

Abstract Hybrid filaments are of growing interest for a wide range of applications, including those that require stimuli-responsiveness. In this study we developed magnetic filaments by combining the properties of inorganic nanoparticles with the low density, flexibility and morphological features of 2,2,6,6-tetramethylpiperidine-1-oxyl (TEMPO)-oxidized cellulose nanofibrils (TOCNF). The hybrid filaments were synthesized by wet spinning of TOCNF using sodium alginate (SA) adjuvant in a hydrogel containing magnetite (Fe_3O_4) nanoparticles (NPs) formed *in-situ* by nucleation and grow. The relationship between synthesis conditions and filament mechanical and magnetic properties were investigated at NP loading as high as 25%. Saturation magnetization of 1.60, 11.31, 19.41, and 33.25 emu/g Fe_3O_4 were measured at 5, 10, 15, and 25% NPs with a penalty in filament tensile strength which nevertheless reached at least 118 GPa along with low magnetite crystal orientation. Such high strength is rarely reported and found to depend on cellulose crystal orientation. The magnetic filaments were found suitable to replace traditional magnetic systems but add to the opportunity to develop flexible microwave adsorption textiles, artificial muscles, and micro-sensors.

Keywords Filaments · Nanocellulose · Wet spinning · Coagulation · Magnetic filaments · Coaxial filaments

Supplementary Information The online version contains supplementary material available at https://doi.org/10.1007/s10570-024-06291-z.

L. de Castro-Alves (✉) · M. A. González-Goméz · P. Garcia-Acevedo · Á. Arnosa-Prieto · Y. Piñeiro-Redondo · J. Rivas
Department of Applied Physics, Nanotechnology and Magnetism Lab — NANOMAG, Materials Institute – iMATUS, Health Research Institute - IDIS, Universidad de Santiago de Compostela, 15782 Santiago de Compostela, Spain
e-mail: lisandracristina.decastro@usc.es

L. Wang (✉) · M. Borghei · O. J. Rojas
Department of Bioproducts and Biosystems, Aalto University, P.O. Box 16300, 00076 Aalto, Finland
e-mail: ling.wang@aalto.fi

M. A. González-Goméz
Nanostructured Materials Group, International Iberian Nanotechnology Laboratory-INL, Av. Mestre José Veiga S/N, 4715-330 Braga, Portugal

O. J. Rojas
Bioproducts Institute, Department of Chemical and Biological Engineering, Department of Chemistry and Department of Wood Science, University of British Columbia, 2360 East Mall, Vancouver, BC V6T 1Z3, Canada

Introduction

Depending on the nature and size of magnetic nanoparticles (MNPs), they show superparamagnetic (SPM), ferromagnetic (Ferro), ferrimagnetic (Ferri), or antiferromagnetic (anti-Ferro) behavior, which are of interest in applications, such as magnetic resonance imaging (MRI), targeted drug delivery and in biological separation (Liao and Chen 2002; Chen et al. 2013; Sahoo et al. 2013). In combination with other substances, MNPs produce versatile multi-functional materials. Of particular interest are magnetite (Fe_3O_4) nanoparticles (NPs) which can be customized in size, shape, and function by incorporating ad hoc designed surface properties (Li et al. 2011; Liu et al. 2013). Moreover, they can be scaled up for industrial production via cost-effective and eco-friendly processes such as coprecipitation (Blaney 2007). Owing to their thermal stability (Li et al. 2011), Fe_3O_4 NPs have a relevant role in diverse applications, including metals separation, data storage media, microwave adsorption, and shape memory (Liu et al. 2005; Schmidt 2006; Yavuz et al. 2006; Mincheva et al. 2008; Li et al. 2011).

Biopolymers such as cellulose, lignin, chitosan or alginate (Verma and Fortunati 2019) can be sourced from residues from the forest, food or marine industries, and represent an alternative to the petroleum-based products. Cellulose, in particular, is found in plant structures composed of ordered and disordered domains and is isolated in the form of cellulose nanocrystals (CNCs) and nanofibrils (CNFs) (Moon et al. 2011). The latter can be produced by chemical, physical, or physicochemical pretreatment methods. Treatment with 2,2,6,6-Tetramethylpiperidine-1-oxyl radical (TEMPO) produces anionic CNFs (referred to TOCNFs) with very small width (3–4 nm) and, at least a few microns in length. TOCNF form lightweight, strong structures that benefit from the presence of carboxylate groups (-COO), which impart electrostatic stabilization (Saito et al. 2009; Isogai et al. 2011; Levanič et al. 2020).

Alginate, extracted from brown seaweeds is composed of β-D-mannuronate (M) and α-L-guluronate (G) units linked in given block sequences (M-M, G-G, and M-G) and is widely used in the pharmaceutical, cosmetic, and food industries. In addition, alginates are considered in environmental remediation due to the effect of gelation, biocompatibility, non-toxicity, adsorption capability and low cost (He et al. 2020).

Hybrid biobased materials, for instance, based on TOCNF and alginates, can achieve unique properties and potential advantages arising from the inorganic phase. The latter contribute to enhanced thermal stability, refractive index, hardness, optical or stimuli responsiveness (Chiellini and Solaro 2003; Khan et al. 2023). Alginates are being used as scaffolding materials to incorporate inorganic NPs or biologically active substance for medical applications due to their porosity and high surface-to-volume ratio (Bhattarai et al. 2006). Likewise, nanocellulose is used as natural bio-template combined with inorganic nanoparticles in the shape of membranes (Zheng et al. 2013), nanopaper (Li et al. 2013), filaments (Wang et al. 2019, 2020), and others (Shi et al. 2013). The resulting materials are known for their excellent conductivity or magnetic properties combined with outstanding mechanical performance and flexibility. The combination of these characteristics can introduce novel stimuli-responsive properties into flexible electrodes, displays, drug release devices or even in implantable biosensors (Shi et al. 2013).

Magnetic filaments, combining the magnetic response of MNPs and the lightness, transparency, and flexibility from biopolymers such as alginate and nanocellulose. Efforts have been made to enhance filaments homogeneity by embedding small (D = 30 nm) SPM NPs in polymeric nanofibers (Wang et al. 2008; Miyauchi et al. 2011; Zhang et al. 2017) via homogenous spinning and extrusion. MNPs and polymeric dispersions have been processed by coaxial spinning (Mincheva et al. 2008), where the polymer solution was placed in the shell and MNPs at the core. Wet spinning, on the other hand, is recognized to produce filaments at industrial scale (Zhou et al. 2017; Kim et al. 2019) and is suitable to produce filaments with a uniaxial orientation that ensures enhanced mechanical performance (Iwamoto et al. 2011; He et al. 2020).

Recently, alginate filaments produced via wet spinning were produced for several applications (Fan et al. 2005, 2007; Sa and Kornev 2011; Zhao et al. 2019). The sodium alginate spinning dope was extruded into a coagulation bath containing $CaCl_2$ to form a filament with sufficient mechanical strength. Alginate has also been blended with other polymers and NPs to improve their properties in

the form of filaments. Recently, alginate filaments were reinforced with cellulose nanofibrils proving a great potential in the biomedical field (Park et al. 2021). The addition of functional NPs, such as gold nanoclusters embedded into alginate filaments, imparts not only high mechanical strength but also fluorescence, opening up possibilities for technological applications as anticounterfeiting label in the textile field (He et al. 2020).

Despite the progress made in the area of filament spinning, the incorporation of SPM NPs with sodium alginate and cellulose nanofibrils is still unexplored. In this work, we introduce the synthesis of Fe_3O_4 NPs by co-precipitation, using both *in-situ* (synthesized in a TOCNF matrix) and *ex-situ* (without TOCNF matrix) methods to prepare magnetic filaments. The effect of MNPs synthesized *in-situ* on the nanofibrils level was accessed. We further investigated the impact of the NP synthesis method and concentrations on the mechanical, magnetic, and morphological properties of the developed magnetic filaments (Mono and Coaxial).

Materials and methods

Materials

All chemicals were used without further purification. Iron (III) chloride hexahydrate ($FeCl_3{\cdot}6H_2O$, 99%) was obtained from Alfa Aesar (Madrid, Spain), iron (II) sulphate heptahydrate ($FeSO_4{\cdot}7H_2O$, 99%), calcium chloride ($CaCl_2$), ammonium hydroxide (NH_4OH, 25 wt%), sodium hydroxide (NaOH), absolute ethanol, and sodium alginate were purchased from Sigma (Saint Louis, MO, USA). Never dried bleached hardwood (birch) pulp was oxidized by 2,2,6,6-tetramethylpiperidine-1-oxyl (TEMPO) at pH 10, then washed with deionized water. The TEMPO-oxidized fibers were further microfluidized through one pass high-pressure microfluidization (Microfluidics Corp., USA), yielding TEMPO-oxidized nanofibrils (TOCNF). The obtained TOCNF (1.6 wt% of dry content) had a carboxylic group content of 0.6 mmol g^{-1}. TOCNF aqueous suspensions were prepared at 1.23% and 2% solid content.

Fe_3O_4 NPs prepared i*n-situ* and *ex-situ*

Fe_3O_4 NPs were synthesized through two methods: *in-situ* synthesis within a suspension of TOCNF, and *ex-situ* (without TOCNF) synthesis via the coprecipitation method. In the *in-situ* method, 5.4 g of $FeCl_3.6H_2O$ and 3.3 g of $FeSO_4.7H_2O$ were added to a 250 mL aqueous suspension containing 40 wt% TOCNF based on the total dry mass. After complete dissolution of the iron salts, the mixture was heated at a constant temperature of 80 °C for approximately 30 min under mechanical stirring and N_2 flow. Thereafter, 15 mL of NH_4OH (25 wt%) was added dropwise, and the solution was continuously stirred for an additional 30 min. The reaction was stopped, allowing the solution to cool to room temperature, followed by thorough rinsing with water and ethanol (using a permanent magnet). The percentage of NPs and TOCNF in dispersion (V = 150 mL) was determined by thermogravimetric analysis (TGA), revealing that 25% of the material comprised NPs, while 20% consisted of TOCNF in solution.

In another method, 15 mL of NaOH (5 M) was used, and different weight ratios of iron salts ranging from 5.4 g – 0.24 g for $FeCl_3.6H_2O$ and from 3.3 g to 0.15 g for $FeSO_4.7H_2O$ were added to obtain various concentrations of NPs in solution (accounting for the loss of NPs during cleaning). This method followed the same procedure as described above, resulting in NP concentrations of 25, 10, and 5%, with 20% TOCNF in each of the magnetic dispersions (V = 150 mL). In all the magnetic *in-situ* dispersions it was added 5.4 g sodium alginate (SA) and were left agitating for 4 h at room temperature. The final magnetic *in-situ* dispersions containing TOCNF, SA, and MNPs, were stored at 4 ºC until their use and were referred as: T20/NP25/SA3.6 (NH_4OH), T20/NP10/SA3.6 (NaOH), T20/NP5/SA3.6 (NaOH), and T20/NP25/SA3.6 (NaOH). The T, NP, and SA are used as abbreviations for the TOCNF (T), nanoparticle (NP), and sodium alginate (SA), respectively, and the corresponding % loading after the latter component is indicated by its percentage in suspension T (20%), NP (25, 10, and 5%) and SA (3.6%). After the label is stated, the reducing agent used in the preparation of the magnetic NPs.

The *ex-situ* preparation of Fe_3O_4 NPs, is basically done following the same procedure as the *in-situ* synthesis using NH_4OH as the reducing agent

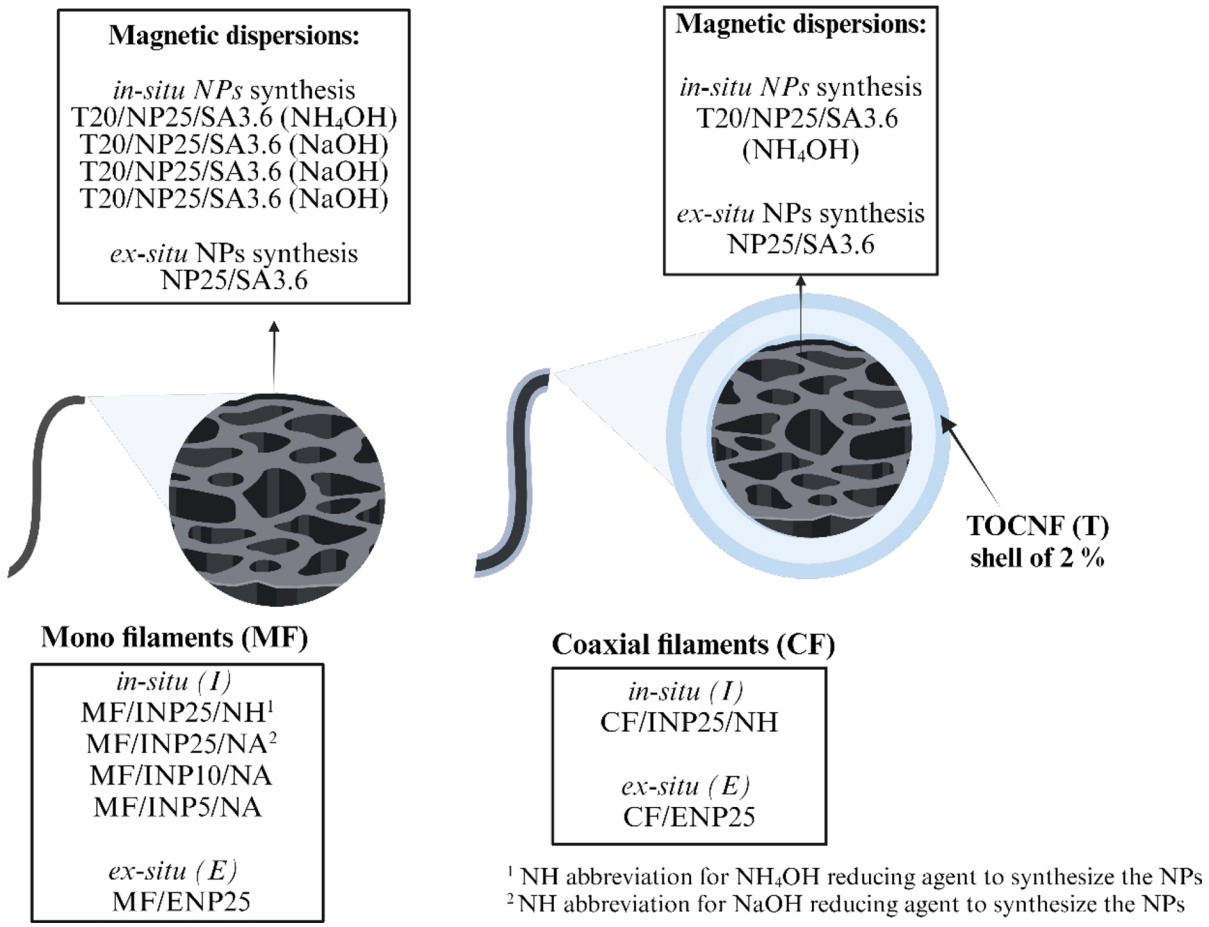

Scheme 1. Magnetic dispersions prepared per type of filaments, Mono (MF) and Coaxial (CF)

in the absence of TOCNF, but with minor differences. The iron salts (5.4 g of $FeCl_3.6H_2O$ and 3.3 g of $FeSO_4.7H_2O$) were added to 80 mL MilliQ. After their complete dissolution, the solution was heated at a constant temperature of 80 °C for approximately 30 min under mechanical stirring and N_2 flow. The reaction was stopped, let to cool down at room temperature, before being cleaned with MilliQ water (using a permanent magnet). The total magnetic content was determined by TGA, and a magnetic dispersion with 25% NPs was prepared in 150 mL MilliQ water. After which it was added 5.4 g of SA and left agitating for 4 h at room temperature. The magnetic *ex-situ* dispersion was also stored at 4 ºC until use, and referred as: NP25/SA3.6 (comprised of 25% NPs and 3.6% SA).

Filament wet spinning

The prepared magnetic dispersions were degassed (3 min, 2500 rpm) via a planetary centrifugal mixer (THINKY ARE-250). The homogenous dispersions were then loaded into a 20 mL plastic syringe attached to a plastic tube (44.5 cm length and 6 mm inner diameter) that ended in a coaxial needle (inner diameter of 1.2 mm, outer diameter of 2.1 mm, and a length of 3.7 cm).

Two types of filaments, mono and coaxial (Scheme 1), were fabricated by immersing the coaxial needle in a coagulation bath (1 M $CaCl_2$) at a fixed spinning rate, 10 mL/min. The filaments remained in the coagulation bath for 20 min to allow time for cross-linking. Subsequently, the filaments underwent

two washing steps with distilled water (first step for 10 min and second step for 20 min) and collected and air dried under fixed ends to prevent shrinkage.

The drying time varied based on the filament type: coaxial filaments with a TOCNF shell (2% dry weight) took approximately 2.5 h to dry, while the mono filaments required approximately 1 h. Mono filaments were prepared from all magnetic dispersions (*in-situ* and *ex-situ*), while only coaxial filaments were prepared using the *in-situ* and *ex-situ* magnetic dispersions of T20/NP25/SA3.6 (NH_4OH) and NP25/SA3.6, respectively. Additionally, besides the magnetic filaments, reference mono and coaxial filaments (without magnetic NPs) were spun.

The magnetic wet-spun mono (M) and coaxial (C) filaments (F) containing the given NP amounts, their *in-situ* (I) and *ex-situ* (E) synthesis method, were therein referred to as MF/INP25/NH, MF/INP25/NA, MF/INP10/NA, MF/INP5/NA, MF/ENP25, CF/INP25/NH, and CF/ENP25 (where the abbreviations refer to MF (mono filament), CF (coaxial filament), INP (*in-situ* nanoparticles), ENP (*ex-situ* nanoparticles), NH (refers to NH_4OH reducing agent), and NA (refers to NaOH reducing agent), respectively).

Nanoparticles and filaments characterization

Filament morphology

The morphology and NP size were assessed by transmission electron microscopy (TEM) by using a JEOL JEM-1011 microscope (JEOL, Tokyo, Japan). Prior to the measurements, a diluted dispersion of each nanoparticle was prepared. Approximately 10 µl of the diluted particle dispersion was deposited onto a copper grid with a thin layer of carbon film (Formvar films) and was left to dry under a white light bulb.

The filaments morphology and cross sections at break were observed by scanning electron microscopy (SEM) using a FESEM ZEISS Ultra plus microscope (Germany) operated at 20 kV with a working distance of 8.5 mm. Before imaging, pieces of the filaments were cut, by bending the frozen filaments in liquid N_2. The filaments were placed horizontally and vertically (cross section images) in 3 nm-Platinum/palladium (Pt/Pd) sputter coater targets. For detection of elements (Fe and C), energy-dispersive X-ray spectroscopy (EDS) spectra were recorded using the high-resolution microscope with the EDS detector (model INCA-X act, Oxford).

Chemical and structural characterization

TOCNF, SA, magnetic dispersions and filaments was evaluated by Fourier transform infrared spectra (FTIR) and recorded on a Varian FT-IR 670 (Varian, Palo Alto, CA, USA) spectrophotometer in of range 400–4000 cm^{-1}. The structural properties were evaluated by X-ray diffraction (XRD) using a Philips PW1710 diffractometer (Panalytical, Callo End, UK), a "PW1820/00" vertical goniometer, and an "Enraf Nonius FR590" generator at 40 kV and 30 mA. The X-rays were obtained from a sealed Cu tube, and the radiation was monochromatized with a graphite monochromator (λ ($K_{\alpha 1}$) = 1.5406 Å. Measurements were collected in the angular range of 10–80° with a step size of 0.02◦ and a step time of 2 s per step. The mean particle size, dispersity (Đ) and zeta potential of the respective component were measured by dynamic light scattering and electrophoretic mobility by using a NanoZS (Malvern Instruments, Malvern, UK) operating at a detection angle of 173°.

Thermal and magnetic properties

The thermal stability of the filaments was recorded by measuring the weight change as a function of temperature in N_2 atmosphere using a Perkin Elmer thermogravimetric analysis unit (TGA) 8000 (Perkin, Waltham, MA, USA). The filaments were milled and heated up from 25 °C to 850 °C at a heating rate of 20 °C/min.

The filaments magnetization was measured using a Vibrating Sample Magnetometer (VSM) (DMS, Massachusetts, MA, USA) at room temperature with a magnetic field ranging from -10,000 to 10,000 Oe. The magnetization values per unit mass were adjusted for the magnetic mass content of each sample, determined through TGA analysis.

Mechanical strength

The mechanical strength of filaments was assessed using an Instron 5944 Single Column tabletop Universal Testing System, operating in tensile mode. Prior to testing, all filaments were conditioned at 23 °C in 50% humidity overnight. The used load cell had a capacity

of 100 N, with a gauge length set to 10 mm with an elongation rate of 0.5 mm/min. The filament diameter was measured using a micrometer (Ironside, graduation 0.001 mm) and at least seven replicates of one sample were measured. The mono magnetic filaments ranged in diameter from approximately 0.07 to 0.15 mm, while the magnetic coaxial filaments from approximately 0.17 to 0.24 mm. The reference mono filaments (without MNPs) measured approximately 0.05 to 0.09 mm in diameter, whereas the reference coaxial filaments measured approximately 0.13 to 0.20 mm.

Surface roughness

The surface topography of the magnetic filaments was evaluated using a 3D Optical Profiler (Sensofar S. Neox) microscope with a white-light vertical scanning interferometry (VSI) mode and CFI60-2 Nikon objective lens of 10×and 50x. The images were processed using the SensoMap software and the following roughness parameters were calculated in multiple areas of each sample: Root mean square roughness (R_q), Total height of profile (R_t), Skewness (R_{sk}), and Kurtosis (R_{ku}) (Gadelmawla et al. 2002).

Wide angle X-ray scattering (WAXS)

WAXS was used to determine the orientation of cellulose and magnetite crystallites in the filaments (Wang et al. 2020). The X-ray intensity data were measured on a Bruker D8 VENTURE PHOTON-III C14 κ-geometry diffractometer system equipped with a Incoatec IμS 3.0 microfocus sealed tube (Cu Kα, λ=1.54178 Å) and a multilayer mirror monochromator. Sample diffraction patterns were collected with a 400 mm sample-to-detector distance and with 200 s waiting time. Before evaluation diffraction patterns were corrected by subtracting the background. Based on azimuthal intensity distribution profiles, the orientation index (π) and Herman's orientation parameter (S) were calculated according to Eq. (1) and Eq. (2) (Nishiyama et al. 1997).

$$\pi = \frac{180° - FWHM}{180°} \tag{1}$$

$$S = \frac{3\left(\cos^2\gamma\right) - 1}{2} \tag{2}$$

where FWHM is the full width at the half-maximum (in degrees) of a peak in the azimuthal intensity distribution profile. The average ($\cos^2\gamma$) is obtained from the average cosine of the azimuthal angle φ based on Eq. (3) and Eq. (4).

$$\left(cos^2\gamma\right) = 1 - 2\left(cos^2\varphi\right) \tag{3}$$

where,

$$\left(\cos^2\varphi\right) = \frac{\sum_{\varphi_0}^{\varphi_0+\pi/2} I(\varphi)\sin\varphi\cos^2\varphi}{\sum_{\varphi_0}^{\varphi_0+\pi/2} I(\varphi)\sin\varphi} \tag{4}$$

where I(φ) is the intensity detected at azimuthal angle φ and φ_0 is the azimuthal angle in the beginning of the range used for the calculation of the average cosine $\langle\cos^2\varphi\rangle$. S was calculated at a φ_0 of 0, π/2, π, and 3π/2, and the average of these values is reported.

Results and discussion

Nanoparticle morphology

The TEM images shown in Fig. 1, illustrate the structure of TOCNF and of Fe_3O_4 NPs synthesized by the different methods and loaded in TOCNF (20%) and SA (3.6%). Figure 1a, shows the web-like like structure of TOCNF with a width size distribution of nanofibrils from 5 to 30 nm.

Figure 1b, shows magnetic dispersion (T20/NP25/SA3.6 NH4OH) with 25% Fe_3O_4 NPs prepared *in-situ,* in the presence of TOCNF (20%) by using NH_4OH as reducing agent. The NPs had a diameter of 7.4 nm, as shown in the respective size distribution histogram. In this magnetic dispersion the NPs are well distinguished within the structure of the nanofibrils.

The TEM images in Fig. 1b to Fig. 1d correspond to the magnetic dispersions (T20/NP25/SA3.6, T20/NP10/SA3.6, and T20/NP5/SA3.6 NaOH) containing 25, 10, and 5% Fe_3O_4 NPs, which were also prepared *in-situ* but using NaOH as a reducing agent. The size histogram of the magnetic dispersions T20/NP25/SA3.6 (NaOH), T20/NP10/SA3.6 (NaOH), and T20/NP5/SA3.6 (NaOH) presented an average diameter size of 7.7, 7.2, and 4.4 nm, respectively.

The TEM images of the magnetic dispersions (NP25/SA3.6) with the NPs synthesized without

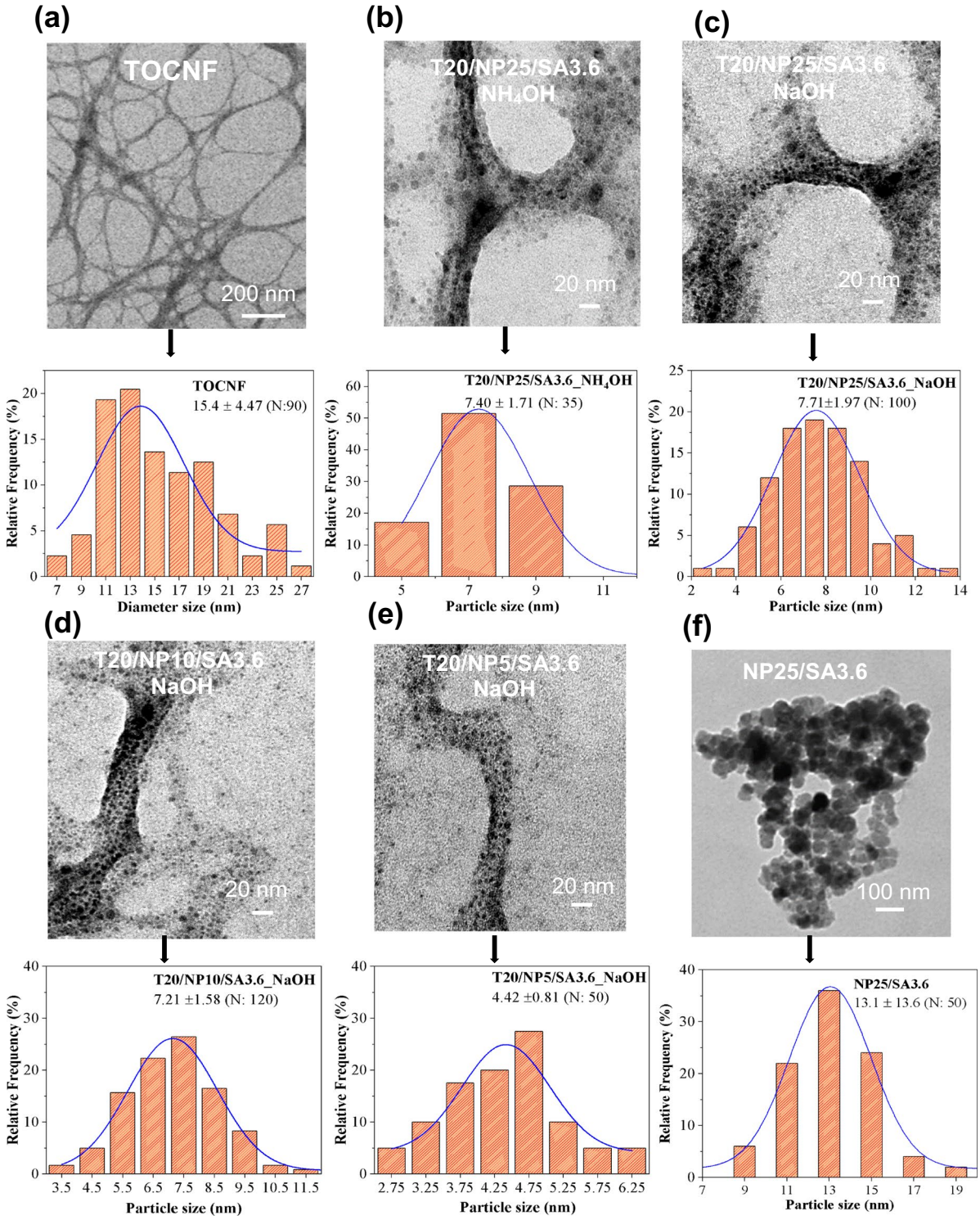

Fig. 1 TEM images of TOCNF **a** and of the magnetic dispersions: T20/NP25/SA3.6_NH$_4$OH **b**, T20/NP25/SA3.6_NaOH **c**, T20/NP10/SA3.6_NaOH **d**, T20/NP5/SA3.6_NaOH **e**, and NP25/SA3.6 **f** (with respective size particle distribution histogram bellow the TEM images)

TOCNF (*ex-situ)* are shown in Fig. 1f. The synthesized NPs showed a size spanning from 9 to 20 nm, and presented a high level of aggregation. Clearly, no differences in the NPs size were observed regarding the reducing agent used. However, the most remarkable difference is that the presence of TOCNF, used in the *in-situ* synthesis, stabilized and allowed better control of NPs size and aggregation. NPs prepared *in-situ,* in the presence of TOCNF, revealed an average diameter of 7 nm while *ex-situ* NPS, presented an average diameter size of about 13 nm, as shown in the size distribution histogram of the magnetic solution NP25/SA3.6. This corroborates that the presence of carboxyl groups in TOCNF stabilize NPs (Uddin et al. 2014). However, although NPs prepared in the presence of TOCNF were smaller, individual NPs remained as part of the supernatant, indicating that not all NPs were integrated with the nanofibers.

Filament characterization

Filament composition and morphology

Mono and coaxial filaments were spun using different MNP concentrations synthesized using the *in-situ (*in the presence of TOCNF*)* and *ex-situ* (absence of TOCNF). The motivation behind the work was to obtain a hybrid inorganic–organic material with unique properties arising from both components. TOCNF presents a gel-like texture and is composed of a matrix of interconnected nanofibrils, as shown in Fig. 2a. The filaments containing TOCNF nanofibrils were dense and rigid, as shown in Fig. 2b.

SEM images in Fig. 3a and Fig. 4a illustrate the surface morphology and respective cross-section at break of the filaments carrying Fe_3O_4 NPs prepared *in-situ* with TOCNF (MF/INP25/NH, CF/INP25/NH, MF/INP25/NA, MF/INP10/NA, and MF/INP5/NA) and *ex-situ* without TOCNF (MF/ENP25 and CF/ENP25), respectively.

All the filaments containing TOCNF showed a relatively rough surface regardless of the MNP preparation method. In contrast MF/ENP25 (Fig. 3a), in the absence of TOCNF, presented a very smooth surface. The cross-section SEM images revealed that all filaments had a circular cross section, but some deformation was observed due to the filaments cryo-cutting in liquid N_2 (Fig. 3a and 4a).

The EDX mapping images and elemental analysis of the filaments cross-section revealed the presence of iron (Fe) (green color) indicating the presence of Fe_3O_4 NPs and carbon (C) element (red color) indicating the presence of either SA and nanocellulose. Iron was heterogeneously dispersed in the mono filaments, MF/ENP25, MF/INP25/NA, MF/INP10/NA, and MF/INP5/NA. However, the three latter filaments displayed a clear reduction of Fe accordingly to the NP concentrations. Regarding the coaxial filaments (CF/INP25/NH and CF/ENP25) an apparent iron core and carbon shell were observed, indicating that TOCNF was uniformly arranged around the magnetic core.

We next measured the surface roughness of the magnetic filaments. Areas of about 0.8 mm^2 from different locations of the samples were scanned, and height variations were recorded. The height and roughness of the profile were determined by ISO

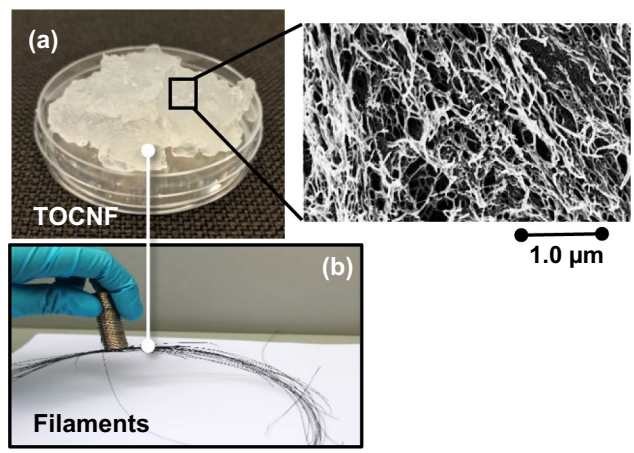

Fig. 2 A photograph of TOCNF **a** and of the prepared magnetic filament CF/INP25/NH **b**

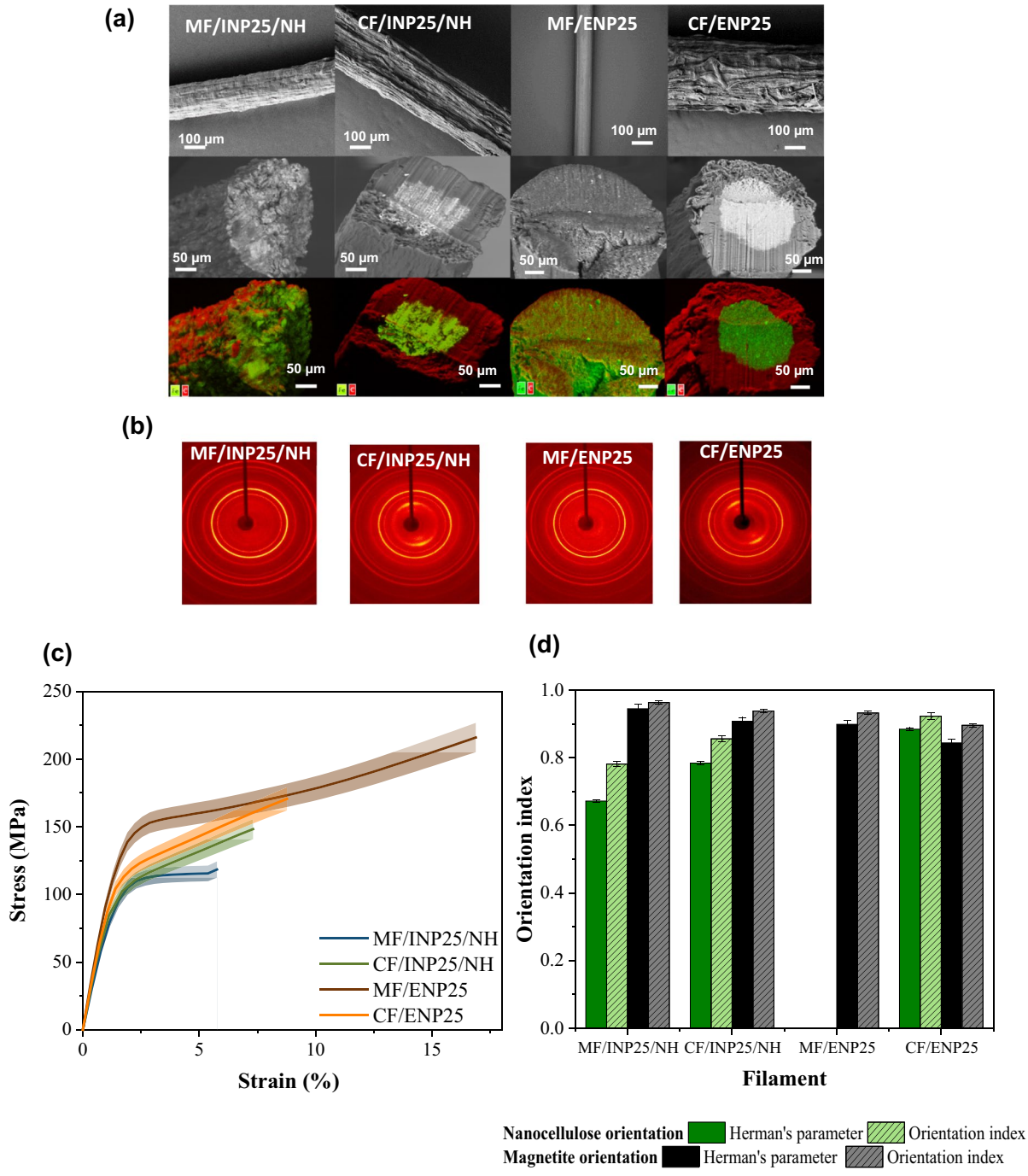

Fig. 3 Main mechanical and structural characteristics of the magnetic filaments MF/INP25/NH, CF/INP25/NH, MF/ENP25, and CF/ENP25: **a** SEM images from cross-sections, **b** Two-dimensional wide-angle X-ray diffraction (2D-WAXS) images, **c** stress and strain curves (the standard deviation is shown as highlighted areas around the different profiles and **d** Nanocellulose fibril and magnetite nanoparticles orientation

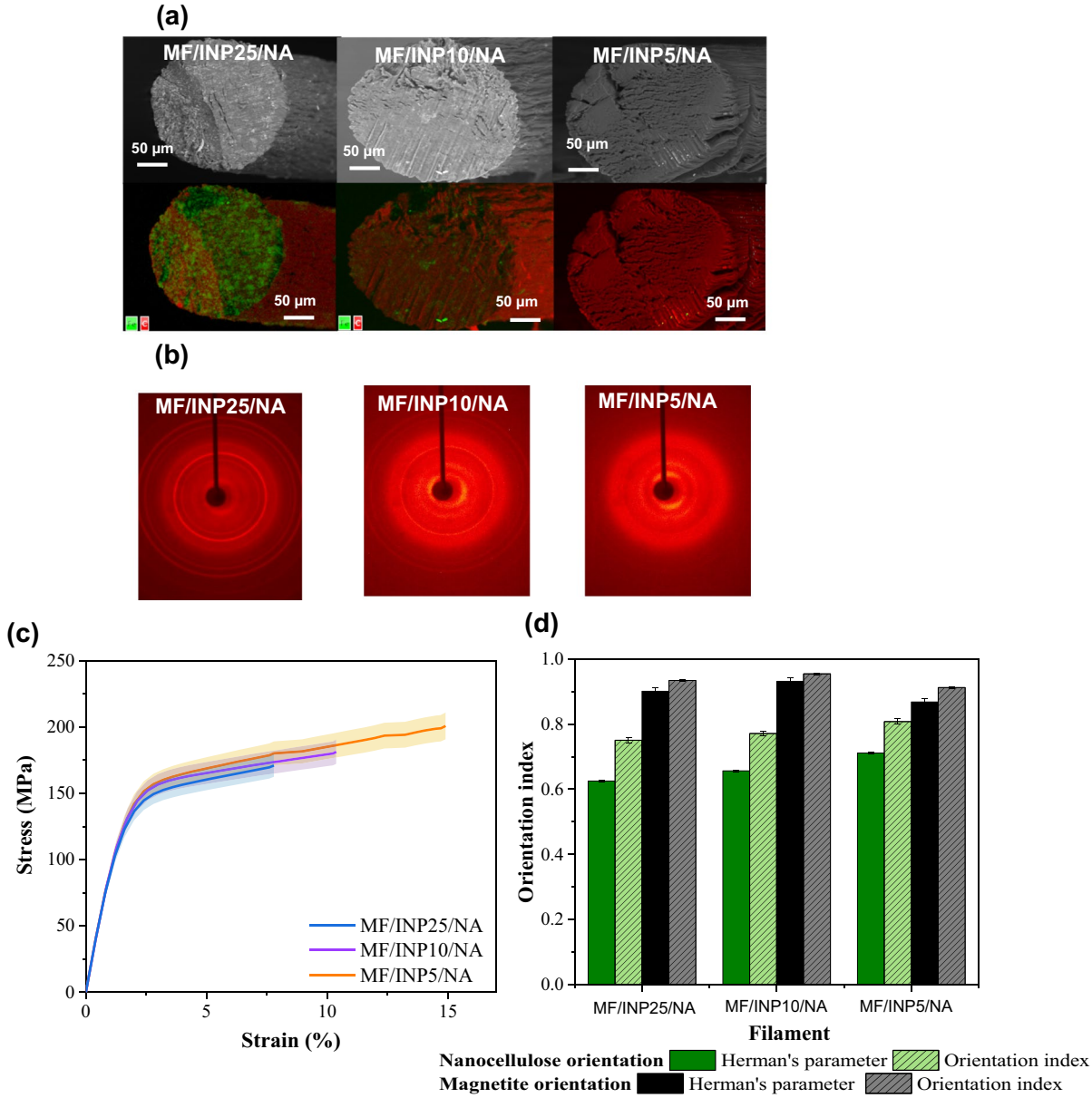

Fig. 4 Main mechanical and structural characteristics of the magnetic filaments MF/INP25/NA, MF/INP10/NA, and MF/INP5/NA: **a** SEM images from cross-sections, **b** Two-dimensional wide-angle X-ray diffraction (2D-WAXS) images, **c** stress and strain curves (the standard deviation is shown as highlighted areas around the different profiles and **d** cellulose fibril and magnetite nanoparticles orientation

4287:1997, and the calculated parameters are presented in Table S1 and 3D images in Figure S1 **(Supporting information)**.

According to the total height (R_t) and roughness (R_q), it is evident that the coaxial filaments (CF/INP25/NH and CF/ENP25) exhibited larger heights and roughness compared with the mono filaments MF/INP25/NH, MF/INP25/NA, MF/INP10/NA, and MF/INP5/NA. Furthermore, the kurtosis (R_{ku}) parameter revealed that the coaxial filaments (CF/INP25/NH and CF/ENP25) presented a more even and uniform surface ($R_{ku} < 3$), while mono filaments

(MF/INP25/NH to MF/INP5/NA) displayed a sharper surface ($R_{ku} > 3$). Nevertheless, the skewness (R_{sk}) parameter showed a positive value in filaments MF/INP25/NA, MF/INP10/NA, MF/INP5/NA, and CF/ENP25, indicating the presence of more peaks on their surface than valleys, in contrast to filaments MF/INP25/NH, CF/INP25/NH, and MF/ENP25. In the end, filaments in which NPs were prepared *in-situ*, in the presence of TOCNF (MF/INP25/NH, MF/INP25/NA, MF/INP10/NA, MF/INP5/NA, and CF/INP25/NH) exhibited higher roughness compared to filaments MF/ENP25 and CF/ENP25, where the NPs were prepared *ex-situ,* in the absence of TOCNF.

Structural and chemical properties

The magnetic filaments were analyzed by XRD and FTIR to assess their structural and chemical characteristics. Figure 5a shows the FTIR spectra of both TOCNF and magnetic filaments. In the TOCNF spectrum, distinctive peaks at 3300 and 2888 cm^{-1} are attributed to the -OH functional group and -CH_2 stretching vibrations of cellulose (Otenda et al. 2022). Furthermore, the vibrational band at 1604 cm^{-1} correspond to -C = O group, while the peaks observed at 1044 and 850 cm^{-1} are associated to C–O–C and β-glycosidic linkage vibrations, respectively (Johar et al. 2012; Otenda et al. 2022). Notably, all the characteristic vibrational peaks of nanocellulose were evident in the FTIR spectra of the magnetic filaments.

The peak corresponding to Fe–O, observed at 565 cm^{-1}, overlapped with a wide peak corresponding to TOCNF. In the case of filaments MF/INP10/NA and MF/INP5/NA, the Fe–O peak was negligible due to the low concentration of Fe_3O_4 NPs (10, 5%) compared to TOCNF (20%) and SA (3.6%), respectively.

Figure 5b, shows the X-ray diffraction of both magnetic filaments and TOCNF. In the diffractogram of TOCNF, two distinct peaks appear at 2Θ = 16.0° and 22.3°, corresponding to the (1–10/110) and (200) diffraction of cellulose I (Xu et al. 2020; French 2014).

These peaks are also present in the diffractogram of the magnetic filaments, indicating the presence of cellulose crystals with varying intensities. Notably, the main peak at 22.3° is more visible in filaments with a TOCNF shell, while the remaining filaments

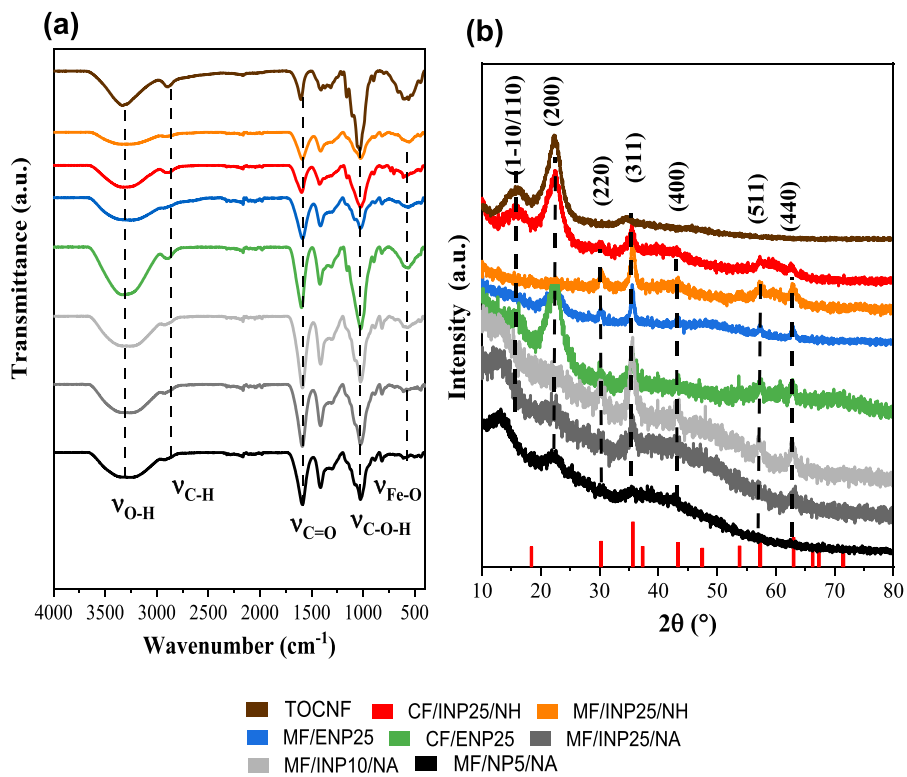

Fig. 5 Infrared **a** spectra and X-ray **b** diffractogram of TOCNF and magnetic filaments (red columns in XRD diffractogram represents the diffraction standard pattern of magnetite

exhibit a broader and less pronounced peak. Additionally, the diffractogram of the magnetic filaments showed diffraction peaks at 2Θ = 30.1, 35.2, 43.2, 57.3, and 62.6° corresponding to the crystallographic planes (220), (311), (400), (511), and (440) of Fe_3O_4 (ICDD: 98–015-8743) (Hastak et al. 2018). The relative intensity of these peaks is correlated with the Fe_3O_4 NP content in the magnetic filaments.

Filaments with NPs prepared in situ, MF/INP25/NH to MF/INP5/NA, showed a decreased intensity and broadening in the main Fe_3O_4 peaks. This suggests that the Fe_3O_4 NPs were small, as observed in TEM, and have a low crystalline quality. This can be attributed to the presence of TOCNF and the coprecipitation procedure.

Mechanical strength and crystallite orientation.

Tensile strength was used to assess the effect of Fe_3O_4 NPs on the mechanical properties of the magnetic filaments. Stress–strain curves of all magnetic filaments are displayed in Fig. 3c and Fig. 4c, respectively. Reference filaments (with no MNPs) revealed a Young's modulus of 10 to 13 (GPa), tensile strength between 210 and 255 (MPa), and a strain at break from 6 to 19%, which are reportedly higher compared to the magnetic filaments (Table S1). Generally, the presence of NPs weakened the mechanical properties of composite materials (Liu and Brinson 2008; Zare 2016).

In this study, at an increased Fe_3O_4 NP content in magnetic filaments from 5 to 25% (MF/INP25/NH, MF/INP25/NA, MF/INP10/NA, MF/INP5/NA), the Young´s modulus, tensile strength and strain at break decreased from 14 to 8 GPa, 201 to 118 MPa, and from 15 to 6%, respectively. This effect can be explained by the reduced covalent/hydrogen bonding occurring between NPs and the negative groups of TOCNF and SA (Oprea and Panaitescu 2020). The presence of MNPs at low concentrations enhanced the mechanical properties of the filaments (Nazari 2017).

For instance, the filaments prepared in the absence of TOCNF (MF/ENP25 and CF/ENP25) tolerated a high tensile strength (216 MPa, 171 MPa), strain at break (17%, 9%), and Young's Modulus (10 GPa, 9 GPa), respectively. The addition of TOCNF shell in CF/ENP25 filament increased the strain at break. More studies are needed to explain this behavior and the optimum concentration of Fe_3O_4 NPs to improve the mechanical performance.

WAXS was performed to investigate cellulose nanofiber and Fe_3O_4 orientation in the filaments. The 2D WAXD patterns of the spun filaments are shown in Fig. 3b and Fig. 4b, respectively. Broad and indistinct rings or arcs were observed in the X-ray patterns, suggesting the presence of some crystallinity in the filaments. However, the haziness of the diffraction rings indicated that the degree of crystallinity was relatively low in the filaments MF/INP25/NA, MF/INP10/NA, and MF/INP5/NA. This is likely due to the molecular segment's heterogeneity along the polymer chain and the lower NP concentration.

The orientation index and Herman's parameter are included in Fig. 3d and Fig. 4d. Both parameters are used as an indicator of cellulose and magnetite crystallite orientation, with 0 and 1 corresponding to complete disorder and fully aligned crystals, respectively. Accordingly, filaments with 25% NPs prepared *in-situ* in TOCNF (MF/INP25/NH and CF/INP25/NH) presented a better alignment of magnetite crystals, as indicated by both the orientation index (0.96 and 0.94) and Herman's parameter (0.95 and 0.91), respectively. However, in filaments MF/INP25/NA, MF/INP10/NA, and MF/INP5/NA, with Fe_3O_4 NP content from 25 to 5% and synthesized with the other method, presented less aligned NPs. The latter filament presented the lowest Herman's parameter (0.87) and orientation index (0.91). The filaments, MF/ENP25 and CF/ENP25, with NPs (25%) prepared *ex-situ,* presented an orientation index of 0.93 and 0.90 and Herman's parameter of 0.90 and 0.84, respectively. MF/ENP25 filament reported the best alignment of magnetite crystals after MF/INP25/NH and CF/INP25/NH filaments.

A higher cellulose crystal alignment was observed in filaments (CF/INP25/NH and CF/ENP25) with TOCNF shell reporting an orientation index of 0.86 and 0.92 and Herman's parameter of 0.78 and 0.88, respectively. Clearly, when the cellulose crystals are aligned in these filaments, the (200) diffraction rings are reduced to arcs and become better defined, indicating better fibril orientation. This is further confirmed by the azimuthal intensity profiles (Fig. S3) where the peaks are sharper. The presence of a TOCNF shell increased the fibril alignment in CF/ENP25 compared to the CF/INP25/NH filament. Moreover, a slight improvement in cellulose fibril orientation was observed in filament MF/INP5/NA (NPs content of 5%), reaching an orientation index

of 0.71 and Herman's parameter or 0.81, compared to MF/INP25/NH, MF/INP25/NA, and MF/INP10/NA which reported an orientation index of 0.75, 0.75, and 0.77 and a Herman's parameter of 0.64, 0.63, and 0.66, respectively.

The magnetite crystal orientation and Young's modulus were correlated, since the filaments presenting a higher Young's modulus had a low crystal orientation. Filaments MF/INP25/NA, MF/INP10/NA, and MF/INP5/NA had a Young's modulus of 9, 11, and 14 GPa, respectively. Meanwhile filaments MF/INP25/NH, CF/INP25/NH, MF/ENP25, and CF/ENP25 presented Young's modulus of 8, 9, 10, and 9 GPa.

Thermal stability and magnetic behavior

TGA measurements were performed to investigate the weight loss, thermal stability and degradation of Fe_3O_4, TOCNF, and SA in the magnetic filaments. Figure 6a shows the TGA curves of all magnetic filaments, which exhibited a three-stage decomposition. The first one (from 100–200 °C) corresponds to elimination of adsorbed water and other volatile components. The second weight loss, between 200 to 450 °C approximately, is due to polymer decomposition of cellulose (around 315 to 400 °C) and SA (around 212 to 426 °C). The third weight loss (around 450 to 800 °C) occurs the degradation

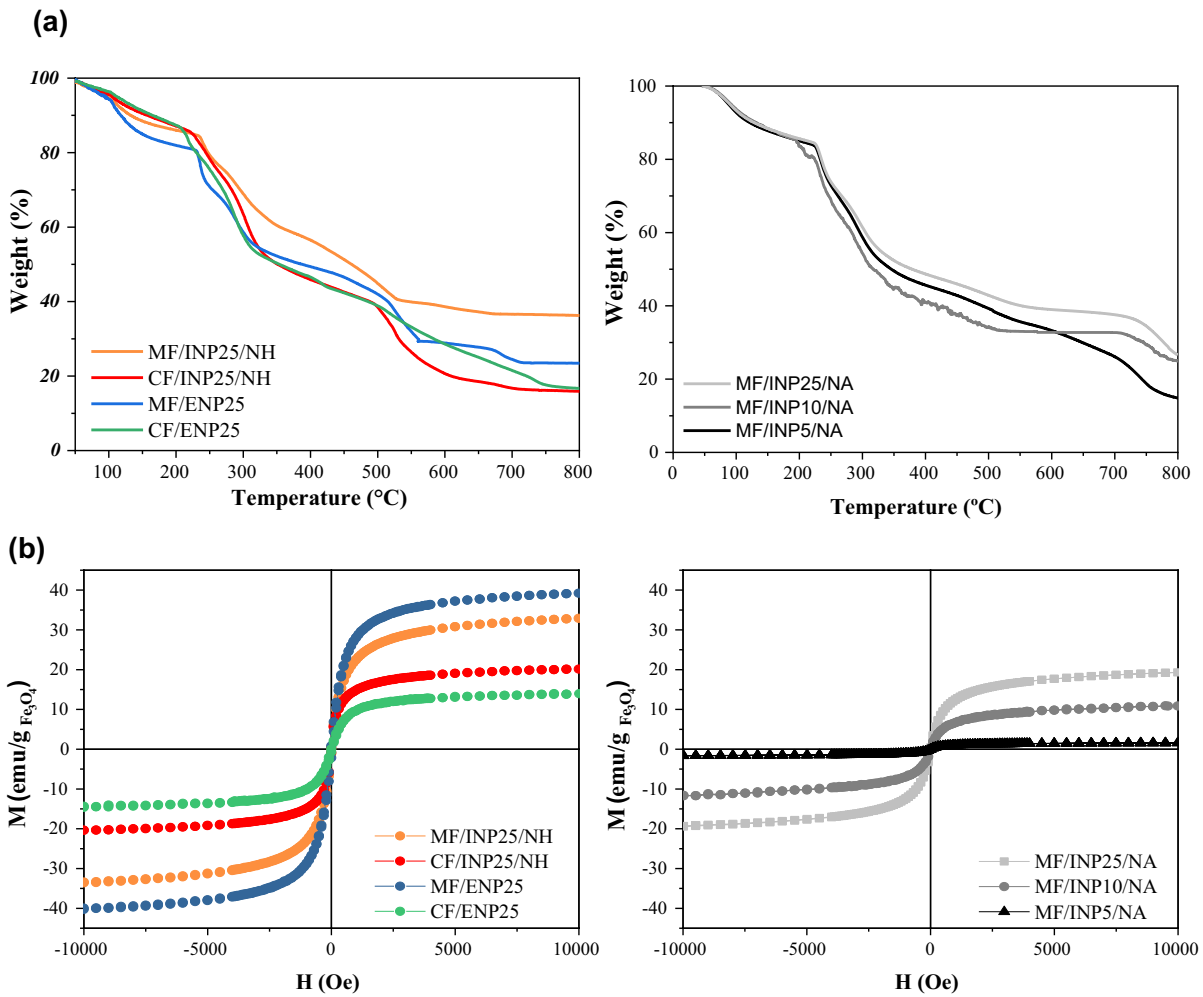

Fig. 6 Thermal stability **a** and magnetization curves **b** of magnetic filaments MF/INP25/NH, MF/ENP25, MF/INP25/NA, MF/INP10/NA, MF/INP5/NA, CF/INP25/NH, and CF/ENP25, respectively

of carbon-based residues. The solid residue that remained above 750 °C corresponds to magnetite, and the amount of magnetic solid content is taken to normalize the magnetization results. This three-stage decomposition is clearly visible in the DTG curves shown in **Fig. S3**, with maximum degradation for the mono filaments occurring around 250 °C and for the coaxial filaments around 315 °C, due to the presence of both biopolymers.

The magnetic properties of the filaments were measured at room temperature using a vibrating sample magnetometer (VSM), with magnetic fields ranging between -10kOe to + 10kOe. The specific magnetization values per unit magnetic mass and their corresponding magnetic solid content (%) are reported in Table S1, and magnetization curves, shown in Fig. 6b. The role of the synthesis procedure is noteworthy. In this study, the coprecipitation method, the *in-situ* preparation of MNPs in the presence of TOCNF using different reducing agents, resulted in Fe_3O_4 NPs with reduced size and low crystallinity, impacting the magnetic properties. Figure 6b, shows the magnetization curves and a reduced magnetization was observed in Fe_3O_4 NPs bonded to TOCNF and SA. This phenomenon aligns with previous research, attributing the magnetization reduction to the encapsulation of MNPs, either by SA or nanocellulose (Denizot et al. 1999; Bedê et al. 2017; Elrhman 2020). Another feature observed is the negligible remnant and coercive force values of the filaments in which the NPs were prepared *in-situ*, in the presence of TOCNF, confirming their superparamagnetic behavior. Moreover, filaments MF/INP25/NA, MF/INP10/NA, and MF/INP5/NA containing Fe_3O_4 NPs prepared in situ (25, 15, and 5%), showed a reduced magnetization, that agrees with the decreased crystalline size and quality of the MNPs, as confirmed by XRD, TEM, and WAXS analyses. The filaments MF/INP25/NH and MF/INP25/NA, even though had the same ratio of Fe_3O_4 NPs (25%), showed differing magnetic properties due to the use of different precipitating agents for MNP synthesis. This difference can be attributed not only to the NPs size but also to differences in crystalline quality, which are influenced by the reactants used (Yazid and Joon 2019; Ba-Abbad et al. 2022). Understanding this complex magnetic behavior lies beyond the scope of this study and additional research is planned in the near future.

Conclusion

Mono and coaxial magnetic filaments were prepared by wet spinning dispersions of TOCNF (20%), SA (3.6%), and MNPs (5–25%). MNPs were synthesized *in-situ* with TOCNF using NH_4OH and NaOH, and *ex-situ* without TOCNF, followed by SA addition. Fe_3O_4 NPs and TOCNF significantly affected the filaments' properties. NPs synthesized with TOCNF were smaller (5–9 nm) and less aggregated. Filament MF/INP25/NH (25% NPs, NH_4OH reducing agent) showed higher magnetization and better crystal alignment than MF/INP25/NA (25% NPs, NaOH reducing agent), while the latter had better mechanical properties. Meanwhile the mono filament without TOCNF, exhibited higher mechanical strength and magnetization but lower crystal alignment and the coaxial filaments (CF/INP25/NH and CF/ENP25) overcame poor orientation and mechanical strength issues. Filaments with TOCNF had a more porous and rougher surface, and high MNP loading reduced density and crystallinity, impacting mechanical strength and thermal stability. These hybrid materials have potential applications in micro-sensors, artificial muscles, flexible microwave absorption textiles, and data storage media, guided by the identified cause-effect relationships.

Author contributions Conceptualization: L.d.C.A., Y.P.R., M. B.; Methodology: L.W.; Formal analysis and investigation: L.d.C.A, L. W., M.A.G.G., P.G.A., A.A.P.; Writing-original draft preparation: L.d.C.A.; Writing-review and editing: L.W, Y.P.R., O.J.R., J.R.; Funding acquisition, Resources, Supervision: O.J.R, J.R.

Funding The authors would like to acknowledge financial support from the Spanish Ministry of Science and Innovation under the grant (PID2020-112626RBC21), in the categories of «Research Challenges» and «Knowledge Generation», the Regional Consellería de Innovacion Program for the Grupos de Referencia Competitiva 2021 – RC2021 project of Xunta de Galicia, the Canada Excellence Research Chair Program (CERC-2018–00006), Canada Foundation for Innovation (Project 38623) and Pacific Economic Development Canada (PacifiCAN).

Data availability No datasets were generated or analysed during the current study.

Declarations

Conflict of interest The authors declare no competing interests.

Ethical approval. Ethics approval was not required for this research.

Consent for publication All authors agreed to the publication in the submitted form.

Open Access This article is licensed under a Creative Commons Attribution-NonCommercial-NoDerivatives 4.0 International License, which permits any non-commercial use, sharing, distribution and reproduction in any medium or format, as long as you give appropriate credit to the original author(s) and the source, provide a link to the Creative Commons licence, and indicate if you modified the licensed material. You do not have permission under this licence to share adapted material derived from this article or parts of it. The images or other third party material in this article are included in the article's Creative Commons licence, unless indicated otherwise in a credit line to the material. If material is not included in the article's Creative Commons licence and your intended use is not permitted by statutory regulation or exceeds the permitted use, you will need to obtain permission directly from the copyright holder. To view a copy of this licence, visit http://creativecommons.org/licenses/by-nc-nd/4.0/.

References

Ba-Abbad MM, Benamour A, Ewis D et al (2022) Synthesis of Fe3O4 Nanoparticles with Different Shapes Through a Co-Precipitation Method and Their Application. JOM 74:3531–3539. https://doi.org/10.1007/S11837-022-05380-3

Bedê PM, da Silva MHP, da Figueiredo AB-H, S, Finotelli PV, (2017) Nanostructured magnetic alginate composites for biomedical applications. Polímeros 27:267–272. https://doi.org/10.1590/0104-1428.2267

Bhattarai N, Li Z, Edmondson D, Zhang M (2006) Alginate-Based Nanofibrous Scaffolds: Structural, Mechanical, and Biological Properties. Adv Mater 18:1463–1467. https://doi.org/10.1002/adma.200502537

Blaney L (2007) Magnetite (Fe3O4): Properties, synthesis, and applications

Chen C, Jiang X, Kaneti YV, Yu A (2013) Design and construction of polymerized-glucose coated Fe3O4 magnetic nanoparticles for delivery of aspirin. Powder Technol 236:157–163. https://doi.org/10.1016/j.powtec.2012.03.008

Chiellini E, Solaro R (2003) Biodegradable Polymers and Plastics. Springer, US, Boston, MA

Denizot B, Tanguy G, Hindre F et al (1999) Phosphorylcholine Coating of Iron Oxide Nanoparticles. J Colloid Interface Sci 209:66–71. https://doi.org/10.1006/jcis.1998.5850

Elrhman HMA (2020) Synthesis and characterization of core-shell magnetite nanoparticles with modified nanocellulose for removal of radioactive ions from aqueous solutions. Results in Materials. https://doi.org/10.1016/j.rinma.2020.100138

Fan L, Du Y, Wang X et al (2005) Preparation and Characterization of Alginate/Poly(Vinyl Alcohol) Blend Fibers. Journal of Macromolecular Science, Part A 42:41–50. https://doi.org/10.1081/MA-200040956

Fan L, Zhu H, Zheng H et al (2007) Structure and properties of blend fibers prepared from alginate and konjac glucomannan. J Appl Polym Sci 106:3903–3907. https://doi.org/10.1002/APP.27088

French AD (2014) Idealized powder diffraction patterns for cellulose polymorphs. Cellulose 21:885–896. https://doi.org/10.1007/s10570-013-0030-4

Gadelmawla ES, Koura MM, Maksoud TMA et al (2002) Roughness parameters. J Mater Process Technol 123:133–145. https://doi.org/10.1016/S0924-0136(02)00060-2

Hastak V, Bandi S, Kashyap S et al (2018) Antioxidant efficacy of chitosan/graphene functionalized superparamagnetic iron oxide nanoparticles. J Mater Sci Mater Med. https://doi.org/10.1007/S10856-018-6163-0

He Y, Du E, Zhou X et al (2020) Wet-spinning of fluorescent fibers based on gold nanoclusters-loaded alginate for sensing of heavy metal ions and anti-counterfeiting. Spectrochim Acta A Mol Biomol Spectrosc 230:118031. https://doi.org/10.1016/j.saa.2020.118031

Isogai A, Saito T, Fukuzumi H (2011) TEMPO-Oxidized Cellulose Nanofibers. Nanoscale 3:71–85. https://doi.org/10.1039/C0NR00583E

Iwamoto S, Isogai A, Iwata T (2011) Structure and Mechanical Properties of Wet-Spun Fibers Made from Natural Cellulose Nanofibers. Biomacromol 12:831–836. https://doi.org/10.1021/bm101510r

Johar N, Ahmad I, Dufresne A (2012) Extraction, preparation and characterization of cellulose fibres and nanocrystals from rice husk. Ind Crops Prod 37:93–99. https://doi.org/10.1016/j.indcrop.2011.12.016

Khan I, Khan I, Saeed K et al (2023) Polymer nanocomposites: an overview. Design, Synthesis, Functionalization, Properties, and Applications, Smart Polymer Nanocomposites. https://doi.org/10.1016/B978-0-323-91611-0.00017-7

Kim S-W, Kwon S-N, Na S-I (2019) Stretchable and electrically conductive polyurethane- silver/graphene composite fibers prepared by wet-spinning process. Compos B Eng 167:573–581. https://doi.org/10.1016/j.compositesb.2019.03.035

Levanič J, Šenk VP, Nadrah P et al (2020) Analyzing TEMPO-Oxidized Cellulose Fiber Morphology: New Insights into Optimization of the Oxidation Process and Nanocellulose Dispersion Quality. ACS Sustain Chem Eng 8:17752–17762. https://doi.org/10.1021/acssuschemeng.0c05989

Li X, Zhang B, Ju C et al (2011) Morphology-controlled synthesis and electromagnetic properties of porous Fe3O4 nanostructures from iron alkoxide precursors. J Phys

Chem C 115:12350–12357. https://doi.org/10.1021/JP2031147Q
Li Y, Zhu H, Gu H et al (2013) Strong transparent magnetic nanopaper prepared by immobilization of Fe3O4 nanoparticles in a nanofibrillated cellulose network. J Mater Chem A Mater 1:15278–15283. https://doi.org/10.1039/C3TA12591B
Liao M-H, Chen D-H (2002) Preparation and characterization of a novel magnetic nano-adsorbent. J Mater Chem 12:3654–3659. https://doi.org/10.1039/b207158d
Liu H, Brinson LC (2008) Reinforcing efficiency of nanoparticles: A simple comparison for polymer nanocomposites. Compos Sci Technol 68:1502–1512. https://doi.org/10.1016/j.compscitech.2007.10.033
Liu F, Cao PJ, Zhang HR et al (2005) Novel Nanopyramid Arrays of Magnetite. Adv Mater 17:1893–1897. https://doi.org/10.1002/adma.200500367
Liu J, Cheng J, Che R et al (2013) Synthesis and microwave absorption properties of yolk-shell microspheres with magnetic iron oxide cores and hierarchical copper silicate shells. ACS Appl Mater Interfaces 5:2503–2509. https://doi.org/10.1021/AM3030432
Mincheva R, Stoilova O, Penchev H et al (2008) Synthesis of polymer-stabilized magnetic nanoparticles and fabrication of nanocomposite fibers thereof using electrospinning. Eur Polym J 44:615–627. https://doi.org/10.1016/j.eurpolymj.2007.11.001
Miyauchi M, Simmons TJ, Miao J et al (2011) Electrospun Polyvinylpyrrolidone Fibers with High Concentrations of Ferromagnetic and Superparamagnetic Nanoparticles. ACS Appl Mater Interfaces 3:1958–1964. https://doi.org/10.1021/am200187x
Moon RJ, Martini A, Nairn J et al (2011) Cellulose nanomaterials review: structure, properties and nanocomposites. Chem Soc Rev 40:3941. https://doi.org/10.1039/c0cs00108b
Nazari A (2017) Treatment of enzymatic wool with Fe3O4 nanoparticles and citric acid to enhance mechanical properties using RSM. J Text Inst 108:1572–1583. https://doi.org/10.1080/00405000.2016.1267601
Nishiyama Y, Kuga S, Wada M, Okano T (1997) Cellulose Microcrystal Film of High Uniaxial Orientation. Macromolecules 30:6395–6397. https://doi.org/10.1021/ma970503y
Oprea M, Panaitescu DM (2020) Nanocellulose Hybrids with Metal Oxides Nanoparticles for Biomedical Applications. Molecules 25:4045. https://doi.org/10.3390/molecules25184045
Otenda BV, Kareru PG, Madivoli ES et al (2022) Cellulose Nanofibrils from Sugarcane Bagasse as a Reinforcing Element in Polyvinyl Alcohol Composite Films for Food Packaging. Journal of Natural Fibers 19:3585–3597. https://doi.org/10.1080/15440478.2020.1848712
Park J-S, Park C-W, Han S-Y et al (2021) Preparation and Properties of Wet-Spun Microcomposite Filaments from Various CNFs and Alginate. Polymers (Basel) 13:1709. https://doi.org/10.3390/polym13111709
Sa V, Kornev KG (2011) A method for wet spinning of alginate fibers with a high concentration of single-walled carbon nanotubes. Carbon N Y 49:1859–1868. https://doi.org/10.1016/j.carbon.2011.01.008
Sahoo B, Devi KSP, Banerjee R et al (2013) Thermal and pH Responsive Polymer-Tethered Multifunctional Magnetic Nanoparticles for Targeted Delivery of Anticancer Drug. ACS Appl Mater Interfaces 5:3884–3893. https://doi.org/10.1021/am400572b
Saito T, Hirota M, Tamura N et al (2009) Individualization of nano-sized plant cellulose fibrils by direct surface carboxylation using TEMPO catalyst under neutral conditions. Biomacromol 10:1992–1996. https://doi.org/10.1021/BM900414T
Schmidt AM (2006) Electromagnetic Activation of Shape Memory Polymer Networks Containing Magnetic Nanoparticles. Macromol Rapid Commun 27:1168–1172. https://doi.org/10.1002/marc.200600225
Shi Z, Phillips GO, Yang G (2013) Nanocellulose Electroconductive Composites Nanoscale 5:3194–3201. https://doi.org/10.1039/C3NR00408B
Uddin KMA, Lokanathan AR, Liljeström A et al (2014) Silver nanoparticle synthesis mediated by carboxylated cellulose nanocrystals. Green Mater 2:183–192. https://doi.org/10.1680/gmat.14.00010
Verma D, Fortunati E (2019) Biopolymer processing and its composites. In: Biomass, Biopolymer-Based Materials, and Bioenergy. Woodhead Publishing, pp 3–23
Wang L, Yu Y, Chen PC et al (2008) Electrospinning synthesis of C/Fe3O4 composite nanofibers and their application for high performance lithium-ion batteries. J Power Sources 183:717–723. https://doi.org/10.1016/j.jpowsour.2008.05.079
Wang L, Ago M, Borghei M et al (2019) Conductive Carbon Microfibers Derived from Wet-Spun Lignin/Nanocellulose Hydrogels. ACS Sustain Chem Eng 7:6013–6022. https://doi.org/10.1021/acssuschemeng.8b06081
Wang L, Borghei M, Ishfaq A et al (2020) Mesoporous Carbon Microfibers for Electroactive Materials Derived from Lignocellulose Nanofibrils. ACS Sustain Chem Eng 8:8549–8561. https://doi.org/10.1021/acssuschemeng.0c00764
Xu J, Deng X, Dong Y et al (2020) High-strength, transparent and superhydrophobic nanocellulose/nanochitin membranes fabricated via crosslinking of nanofibers and coating F-SiO2 suspensions. Carbohydr Polym. https://doi.org/10.1016/j.carbpol.2020.116694
Yavuz CT, Mayo JT, Yu WW et al (1979) (2006) Low-Field Magnetic Separation of Monodisperse Fe 3 O 4 Nanocrystals. Science 314:964–967. https://doi.org/10.1126/science.1131475
Yazid NA, Joon YC (2019) Co-precipitation synthesis of magnetic nanoparticles for efficient removal of heavy metal from synthetic wastewater. In: AIP Conference Proceedings. American Institute of Physics Inc., p 020019
Zare Y (2016) Study of nanoparticles aggregation/agglomeration in polymer particulate nanocomposites by mechanical properties. Compos Part A Appl Sci Manuf 84:158–164. https://doi.org/10.1016/j.compositesa.2016.01.020
Zhang H, Xia JY, Pang XL et al (2017) Magnetic nanoparticle-loaded electrospun polymeric nanofibers for tissue engineering. Mater Sci Eng, C 73:537–543. https://doi.org/10.1016/j.msec.2016.12.116
Zhao Z, Geng C, Zhao X et al (2019) Preparation of CdTe/Alginate Textile Fibres with Controllable Fluorescence Emission through a Wet-Spinning Process and Application in

the Trace Detection of Hg2+ Ions. Nanomaterials 9:570. https://doi.org/10.3390/nano9040570

Zheng Y, Yang J, Zheng W et al (2013) Synthesis of flexible magnetic nanohybrid based on bacterial cellulose under ultrasonic irradiation. Mater Sci Eng, C 33:2407–2412. https://doi.org/10.1016/J.MSEC.2013.02.007

Zhou G, Byun J-H, Oh Y et al (2017) Highly Sensitive Wearable Textile-Based Humidity Sensor Made of High-Strength, Single-Walled Carbon Nanotube/Poly(vinyl alcohol) Filaments. ACS Appl Mater Interfaces 9:4788–4797. https://doi.org/10.1021/acsami.6b12448

Publisher's Note Springer Nature remains neutral with regard to jurisdictional claims in published maps and institutional affiliations.